

https://doi.org/10.1070/QEL16581

Optical nonlinear properties and dynamics of interband transitions in multilayer MoS_2 structures under femtosecond excitation at a wavelength of 514 nm

D.V. Khudyakov, A.A. Borodkin, D.D. Mazin, A.S. Lobach, S.K. Vartapetov

Abstract. **The optical nonlinear absorption and bleaching of aqueous suspensions of multilayer MoS_2 sheets (structural modification 2H) under excitation by a 400-fs pulse at a wavelength of 514 nm is investigated using longitudinal scanning. The sample exhibits nonlinear absorption at intensities up to 15 GW cm^{-2}, while a further increase in intensity to 70 GW cm^{-2} causes nonlinear bleaching with a relative change in transmission to 14%. The dynamics of interband transitions in the picosecond range is studied by femtosecond laser photolysis. The relaxation time of photoexcited excitons is measured to be 20 ± 2 ps. The transition dynamics is calculated in the three-level approximation, and the absorption cross sections of photoinduced electron transitions from the valence band to the conduction band and from the first to the second conduction band are estimated. It is shown that the optical nonlinear properties of suspensions of multilayer 2H MoS_2 sheets are mainly determined by the dynamics of single-photon interband transitions.**

Keywords: *dichalcogenides of transition metals, two-dimensional semiconductors, single- and multilayer MoS_2 structures, nonlinear optical absorption, relaxation dynamics of photoexcited charge carriers, femtosecond laser photolysis.*

1. Introduction

Transition metal dichalcogenides (TMDs), being two-dimensional semiconductors, are promising for application in film optoelectronics and integrated optics as materials for micro-oscillators, microdetectors, thin-film lasers, and light cavities [1]. In contrast to graphene (another two-dimensional material), TMDs have a band gap in the visible region; this feature can be used to design optoelectronic devices: light-emitting diodes, solar cells, and highly sensitive light detectors. Single- and multilayer MoS_2 structures, which are best-studied TMDs, have a large nonlinear optical response [2–5]. *Q*-switching [6] and mode locking [7] for pulsed generation have been implemented using saturable absorbers based on MoS_2 films. Methods of mechanical and chemical exfoliation of crystalline MoS_2, which are used to fabricate single- and multilayer submicron flakes (in particular, flakes of different geometries), make it possible to change the nonlinear response in wide limits [8]. Despite a large number of experimental studies in this subject, the relaxation dynamics of photoexcited carriers has been studied scarcely, as well as the mechanism of nonlinear optical absorption in single- and multilayer MoS_2 structures. Therefore, additional studies should be performed to design light modulators based on MoS_2 structures.

D.V. Khudyakov, A.A. Borodkin, D.D. Mazin, S.K. Vartapetov Physics Instrumentation Center, A.M. Prokhorov General Physics Institute, Russian Academy of Sciences, Troitsk, 108840 Moscow, Russia; e-mail: dimakh65@gmail.com;
A.S. Lobach Institute of Problems of Chemical Physics, Russian Academy of Sciences, prosp. Akad. Semenova 1, 142432 Chernogolovka, Moscow region, Russia

Received 24 November 2017
Kvantovaya Elektronika **48** (2) 124–128 (2018)
Translated by Yu.P. Sin'kov

2. Experimental

A stable suspension of multilayer MoS_2 sheets (structural modification 2H) in water was prepared using water-soluble polymer carboxymethylcellulose (CMC) (CMC sodium salt of medium viscosity; Sigma). The suspension was prepared by dispersion of a weight of 2H MoS_2 powder in a CMC aqueous solution with a concentration of 1 wt % in an ultrasonic bath (Bandelin sonorex; power 80 W, frequency 35 kHz) for 1 h at room temperature and then processed by an ultrasonic probe disperser (UZDN-1, frequency 35 kHz, power 500 W, probe face diameter 15 mm) in a thermostated steel vessel at a temperature of 24 °C for 8 h. The product of black colour was centrifuged at an acceleration of 5000*g* for 30 min (Eppendorf 5084 centrifuge) to remove large aggregates of MoS_2 particles. The upper part (~80%) of the homogeneous suspension above the precipitate was decanted, diluted in a ratio of 1 : 5 by a CMC aqueous solution (1 wt %). The final product (dark-brown, exhibiting the Tyndall effect, and stable for more than 1 yr) was used in experiments.

The absorption spectrum of the suspension, measured by a Shimadzu UV-3101 PC UV-Vis-NIR scanning spectrophotometer, is shown in Fig. 1. The optical spectrum has four absorption bands peaking at wavelengths of λ = 666, 608, ~440, and 395 nm, which correspond to the A, B, C, and D absorption lines of MoS_2. The MoS_2 concentration in the suspension (0.027 mg mL^{-1}) was determined by measuring the optical absorptance A at λ = 666 nm, using the relation $A = \alpha lC$, where l is the optical path length (in m); C is the concentration of dispersed material (in mg mL^{-1}); and α is the absorption coefficient, equal to ~3400 mL mg^{-1} m^{-1} at λ = 666 nm for suspensions of MoS_2 sheets [9].

The Raman spectrum of a 2H MoS_2 film on glass [dried drop of 2H MoS_2 suspension in CMC aqueous solution (1 wt %)] is presented in Fig. 2. Measurements were performed on a T64000 spectrometer (Horiba Jobin Yvon) with a 100× objective at laser power on the sample of 0.1 mW and λ = 514 nm. The spectrum contains two bands, which correspond

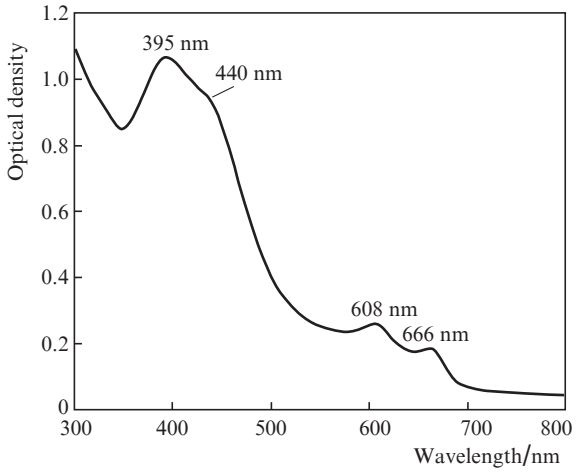

Figure 1. Absorption spectrum of a 2H MoS_2 suspension [0.027 mg mL^{-1} 2H MoS_2 in an aqueous CMC solution (1 wt %); the cell thickness is 2 mm].

to the Raman modes E^1_{2g} and A_{1g}, peaking at frequencies of 383.1 and 407.4 cm^{-1}, respectively. The frequency difference is 24.3 cm^{-1}, a value corresponding to 4–5 layers of MoS_2 nanoparticles (this difference is 25.7 cm^{-1} for the initial MoS_2 powder) [10]. Similar spectra were observed for a MoS_2 suspension in an aqueous solution of polyvinyl alcohol [11].

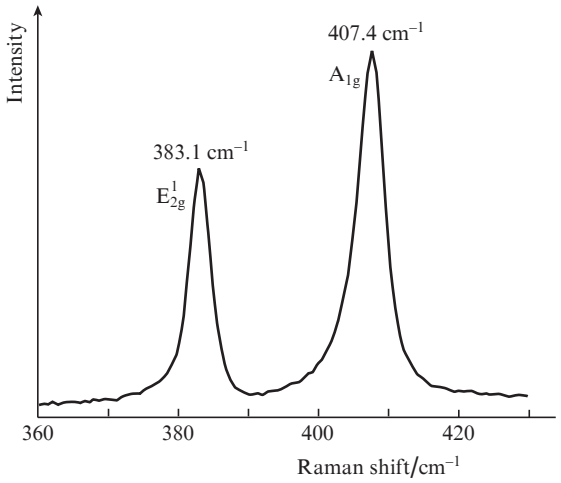

Figure 2. Raman spectrum of a 2H MoS_2 suspension film on glass.

The nonlinear optical characteristics of MoS_2 aqueous suspensions were measured by experimental *P*- and *z*-scan techniques. A schematic of the experimental setup is presented in Fig. 3. A 400-fs pulsed Yb^{3+}:KGW laser with λ = 1028 nm was used for probing in both techniques. The pulse repetition frequency was 1 kHz, and the energy in each pulse was 100 μJ at the fundamental wavelength. The second-harmonic conversion occurred in a KDP crystal with an efficiency of 15%. Longitudinal scanning (*z*-scan measurement) was performed at the second-harmonic wavelength (514 nm) using a conventional scheme without a diaphragm (to detect only nonlinear absorption). The laser beam was focused by a lens L having a focal length of 24 cm. The laser-beam diameter was measured at several points along the scanning coordinate, and the dependence obtained was approximated to determine the exact position of the beam waist and the beam diameter at the focal point. The waist diameter at a level of e^{-2} for the lens L was found to be 110 μm. The sample (a 2-mm-thick cell with a MoS_2 aqueous suspension) was installed on a movable carriage, which could be displaced along the laser beam (i.e., along the *z* axis) near the focal region. The average power P_1 of the radiation transmitted through the sample was recorded by a photodiode in the detection channel. The radiation power incident on the sample (P_2) was measured using a photodiode in the reference channel. The photodiodes were calibrated (using an Ophir power meter) before each experiment. The incident peak intensity I_0 in the beam waist was calculated from the formula

$$I_0 \approx \frac{E}{\pi r_0^2 \tau}, \tag{1}$$

where E is the laser pulse energy incident on the sample, r_0 is the waist radius at a level of e^{-2}, and τ is the laser pulse FWHM. When moving the sample along the *z* axis, the intensity I on the sample surface gradually changed according to the law

$$I(z) = \frac{I_0}{1 + (z/z_0)^2}, \tag{2}$$

where $z_0 = \pi r_0^2/\lambda$ is the Rayleigh length. A neutral filter F at the output of the second-harmonic crystal made it possible to vary the light pulse energy E at λ = 514 nm in the range from one to several microjoules.

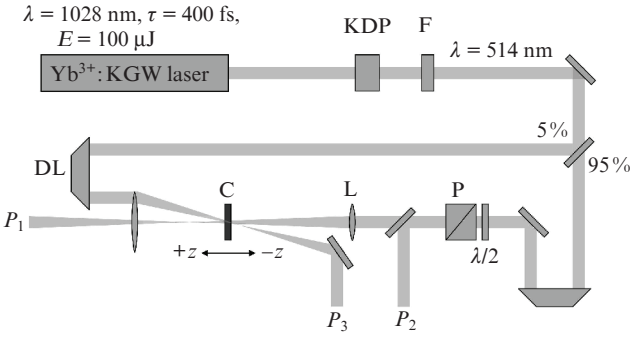

Figure 3. Schematic of the setup for studying the optical nonlinear properties by methods of *z*- and *P*-scan measurements and femtosecond laser photolysis: (KDP) crystal for second-harmonic conversion; (F) spectral filter (and neutral filter attenuating the light power); (DL) delay line; (C) cell with sample; (L) lens; (P) Glan–Thomson prism; (λ/2) half-wave phase plate.

In the case of *P*-scan measurements, the sample was located exactly in the laser beam waist. The pump power density was gradually changed by rotating a half-wave plate installed before a Glan–Thomson prism. The transmittance (ratio of the average power transmitted through the sample to the average power incident on it) was measured in this experiment.

When carrying out femtosecond laser photolysis, the sample was located near the beam waist to obtain desired excita-

tion pulse intensity. A probe pulse, attenuated by a factor of 50 with respect to the excitation one, passed through the excitation region with some time delay, and the average power P_3 of the probe radiation was recorded by a photodiode. The probe pulse delay with respect to the excitation pulse was controlled by the delay line DL.

3. Simulation of experimental data

The dependences of the nonlinear absorption of the sample under our experimental conditions were theoretically estimated using the three-level scheme presented in Fig. 4. This scheme was chosen based on the calculations of the exciton states for 2H MoS_2 [12, 13]. Here, the exciton absorption line B corresponds to the transition from the valence-band state Γ_1^+ to the conduction band state Γ_3^+, from where a transition to the upper conduction band state Γ_1^+ may occur. The gaps between the states approximately correspond to the second-harmonic photon energy (which was used in the experiments): 2.4 eV. The changes in the electron concentrations N_0, N_1, and N_2 at the levels of the valence band (VB), the first conduction band (CB1), and the second conduction band (CB2), respectively, upon excitation by a femtosecond pulse with an intensity $I(t)$ were described by the system of differential equations

$$\frac{dN_0}{dt} = -\frac{\sigma_0 N_0}{h\nu} I + \frac{N_1}{\tau_1} - \frac{\beta}{2h\nu} I^2, \tag{3}$$

$$\frac{dN_1}{dt} = \frac{\sigma_0 N_0}{h\nu} I - \frac{\sigma_1 N_1}{h\nu} I - \frac{N_1}{\tau_1} + \frac{N_2}{\tau_2}, \tag{4}$$

$$\frac{dN_2}{dt} = \frac{\sigma_1 N_1}{h\nu} I - \frac{N_2}{\tau_2} + \frac{\beta}{2h\nu} I^2, \tag{5}$$

where σ_0 and σ_1 are the absorption cross sections of the transitions between the VB and conduction band and between CB1 and CB2, respectively; β is the two-photon absorption coefficient; and τ_1 and τ_2 are the electron lifetimes at CB1 and CB2 levels. The dependence of the sample absorption on the interaction depth is described by the equation

$$\frac{dI}{dz} = -\sigma_0 N_0 I - \sigma_1 N_1 I - \beta I^2. \tag{6}$$

This equation was solved by the iterative method. The sample was divided into M layers so as to provide only slight variation in the femtosecond pulse intensity within each layer at each instant:

$$F_n - F_{n+1} = -(z_{n+1} - z_n) \times \int_{-\Delta t}^{\Delta t} [\sigma_0 N_{0n} I_n + \sigma_1 N_{1n} I_n + \beta^2 (I_n)] dt, \tag{7}$$

where F_n is the photon fluence at the input of the nth layer, $z_{n+1} - z_n$ is the thickness of the nth layer, N_{0n} and N_{1n} are the time-dependent electron concentrations in the VB and the CB1 of the nth layer upon excitation by a pulse with a time intensity profile $I_n = I_{0n}\exp(-t^2/\tau^2)$, and $I_{0n} = F_n/(\sqrt{\pi}\tau)$ is the peak pulse intensity incident on the nth layer. The integration in expression (7) is performed over the time interval from $-\Delta t$ to Δt, within which the pulse intensity is nonzero. The initial

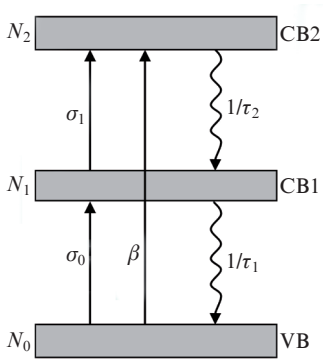

Figure 4. Schematic of the energy bands and transitions in the 2H MoS_2 structure, which was used to describe experimental dependences.

conditions for solving the system were as follows: $N_1 = N_2 = 0$ and $N_0 = 5 \times 10^{16}$ cm^{-3}.

The time-dependent sample transmittance T for a probe pulse is determined by the time dependences of the concentrations N_0 and N_1:

$$T(t) = \frac{I_1}{I_0} \propto \exp\{-[\sigma_0 N_0(t) + \sigma_1 N_1(t)]L\}, \tag{8}$$

where I_1 is the probe pulse intensity transmitted through the sample and L is the sample thickness. Immediately after the pulsed excitation the variation dynamics of N_0 and N_1 is determined by only the interband and intraband relaxation times τ_1 and τ_2 (here, $\tau_1 \gg \tau_2$ [14]). Hence, the picosecond variation kinetics of the signal transmittance in femtosecond laser photolysis is mainly determined by the relaxation time τ_1.

4. Results and discussion

The experimental z- and P-scan curves (Figs 5, 6) showed the same dependence of optical sample transmittance on the peak incident intensity. The sample exhibits nonlinear absorption at incident radiation intensities up to 15 GW cm^{-2}. A further increase in intensity leads to nonlinear clearing of the sample with a relative change in transmittance of 14%. A rise in intensity 70–80 GW cm^{-2} causes sample destruction or boiling.

The excitation pulse intensity on the sample in femtosecond laser photolysis was taken to be 17 GW cm^{-2}; under these conditions, we observed preferred nonlinear absorption

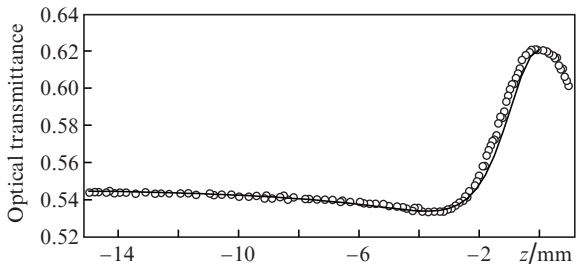

Figure 5. Experimental z-scan signal (left half-wave) and its theoretical approximation.

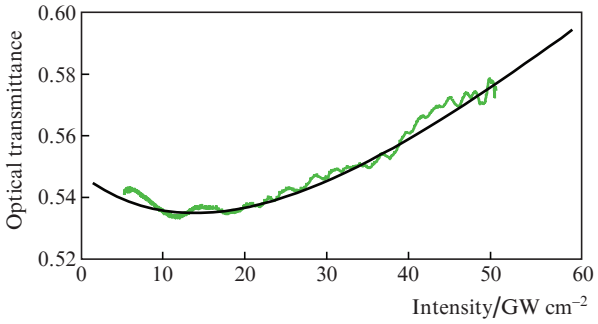

Figure 6. Experimental *P*-scan signal and its theoretical approximation.

related to the variation dynamics of electron concentration in the VB and CB1 states. Using expressions (3)–(5) and (8) to approximate the signal in Fig. 7, one can estimate the photoexcited exciton lifetime: $\tau_1 = 20 \pm 2$ ps.

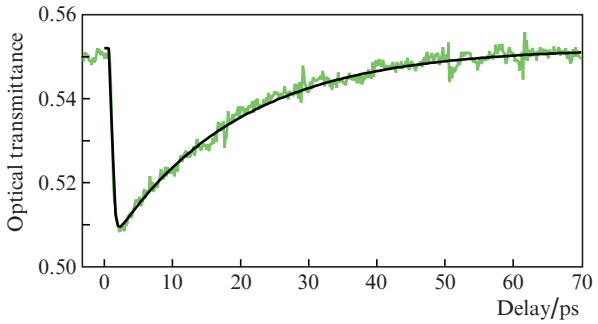

Figure 7. Experimental signal of femtosecond laser photolysis and its theoretical approximation.

A further analysis of the curves in Figs 5 and 6 with the aid of expressions (3)–(5), (7) and the found value of relaxation time τ_1 made it possible to determine the absorption cross sections $\sigma_0 = (6 \pm 1.2) \times 10^{-17}$ cm^2 and $\sigma_1 = (8.3 \pm 1.7) \times 10^{-17}$ cm^2 for the VB–CB1 and CB1–CB2 transitions, respectively. An approximation of the experimental curves allows one to conclude that there is not any significant contribution of two-photon absorption to the *z*- and *P*-scan signals and yields the following estimate from above for the two-photon absorption coefficient: $\beta < 10^{-12}$ cm W^{-1}. This fact explains the significant nonlinear bleaching of the sample even at high excitation intensities. The same absence of significant contribution of two-photon absorption was recorded in solutions of multilayer MoS_2 structures fabricated by chemical and hydrothermal exfoliation of crystalline MoS_2 upon excitation by 100-fs pulses at $\lambda = 800$ nm [14] and 400 nm [15]. To approximate satisfactorily the experimental curves, the intraband relaxation time τ_2 was chosen to be 200 fs.

Thus, an analysis of experimental signals within the three-level approximation suggests that the nonlinear absorption of MoS_2 sample at intensities up to 15 GW cm^{-2} is related to the occupation of CB1 by electrons and absorption on the CB1–CB2 transition. The nonlinear bleaching of the sample at high intensities is due to the occupation of CB2 by electrons and depletion of lower bands: VB and CB1. The measured absorption cross sections of the transitions from the VB and conduction band are of the same order of magnitude as the values found in [3, 8, 14]. However, the σ_1/σ_0 ratio found by us (1.38) is much larger than that obtained in [8]. As far as we know, the exciton pair lifetime τ_1 for suspensions of multilayer MoS_2 structures excited by a femtosecond pulse at $\lambda = 514$ nm, was determined by us directly for the first time. The measured lifetime τ_1 is below 70 ps, a value obtained by measuring the photoluminescence decay of MoS_2 monolayer at $\lambda = 600$ nm upon excitation by a picosecond pulse at $\lambda = 402$ nm [16], and shorter than 100 ps, a value found by measuring the photoexcited exciton lifetime in two- and three-layer samples excited by a femtosecond pulse at $\lambda = 390$ nm and probing at $\lambda = 660$ nm [17]. A possible cause of this inconsistency is the decrease in the recombination time of photoexcited carriers with an increase in the number of layers in multilayer MoS_2 structures. The transition of electrons from the VB to the conduction band in multilayer MoS_2 structures is known to be indirect [18], in contrast to single-layer structures. In this case, the exciton recombination occurs nonradiatively through recombination traps and impurity centres, which transfer the phonon momentum to the lattice. An inhomogeneous concentration of these impurity centres or defects in the lattice may lead to different relaxation times of photoexcited excitons. At the same time, the difference in the relaxation times in different experiments may be related to the detection of excitons of different types when probing at different wavelengths.

Note that, concerning the prospects of application of multilayer MoS_2 structures at intensities below 15 GW cm^{-2}, they behave as reverse saturable absorbers and can be used as nonlinear light beam limiters with a picosecond response time. At high (several tens of GW cm^{-2}) intensities below the destruction threshold, the sample exhibits significant nonlinear bleaching, which can be used in pulsed-laser *Q* switches.

5. Conclusions

The nonlinear optical properties and rates of interband electron transitions in samples of aqueous suspensions of multilayer 2H MoS_2 sheets (4–5 layers) upon photoexcitation by a femtosecond pulse at $\lambda = 514$ nm were investigated. The electron relaxation time from the conduction band to the valence band was measured directly. Two nonlinear transmission regions were found for different ranges of incident light intensity: a reverse-saturation absorption region and a region of significant nonlinear bleaching. The revealed nonlinear optical properties can be used in picosecond light modulators.

References

1. Jariwala D. et al. *ACS Nano*, **8**, 1102 (2014).
2. Zhang M., Howe R., Woodward R., Kelleher E.J.R., Torrisi F., Hu G., Popov S.V., Taylor J.R., Hasan T. *Nano Res.*, **8**, 1522 (2015).
3. Ouyang Q.Y., Yu H.L., Zhang K., Chen Y. *J. Mater. Chem. C*, **2**, 6319 (2014).
4. Xia H., Li H., Lan C., Li C., Zhang X., Zhang S., Liu Y. *Opt. Express*, **22**, 17341 (2014).
5. Woodward R.I., Hasan T., Kelleher E.J.R. *Optoelectronics and Communications Conference (OECC 2015)*. doi: 10.1109/OECC.2015.7340109.
6. Cheng C., Liu H., Shang Z., et al. *Opt. Mater. Express*, **6**, 367 (2016).

7. Liu H., Luo A., Wang F., et al. *Opt. Lett*., **39**, 4591 (2014).
8. Li Y., Dong N., Zhang S., Zhang X., Feng Y., Wang K., Zhang L., Wang J. *Laser Photonics Rev*., **9**, 427 (2015).
9. Coleman J.N., Lotya M., O'Neill A., et al. *Science*, **331**, 568 (2011).
10. Li D., Xiong W., Jiang L., et al. *ACS Nano*, **10**, 3766 (2016).
11. Liu H., Luo A.-P., Wang F.-Z., et al. *Opt. Lett*., **39**, 4591 (2014).
12. Bromley R.A., Murray R.B., Yoffe A.D. *J. Phys. C: Solid State Phys*., **5**, 759 (1972).
13. Beal A.R., Knights J.C., Liang W.Y. *J. Phys. C: Solid State Phys*., **5**, 3540 (1972).
14. Wang K., Wang J., Fan J., Lotya M., et al. *ACS Nano*, **7**, 9260 (2013).
15. Zhang H., Lu S.B., Zheng J., Du J., Wen S.C., Tang D.Y., Loh K.P. *Opt. Express*, **22**, 7249 (2014).
16. Korn T., Heydrich S., Hirmer M., Schmutzler J., Schüller C. *Appl. Phys. Lett*., **99**, 102109 (2011).
17. Wang R., Ruzicka B.A., Kumar N., Bellus M.Z., Chiu H.-Y., Zhao H. *Phys. Rev. B*, **86**, 045406 (2012).
18. Mak K.F., Lee C., Hone J., Shan J., Heinz T.F. *Phys. Rev. Lett*., **105**, 136805 (2010).